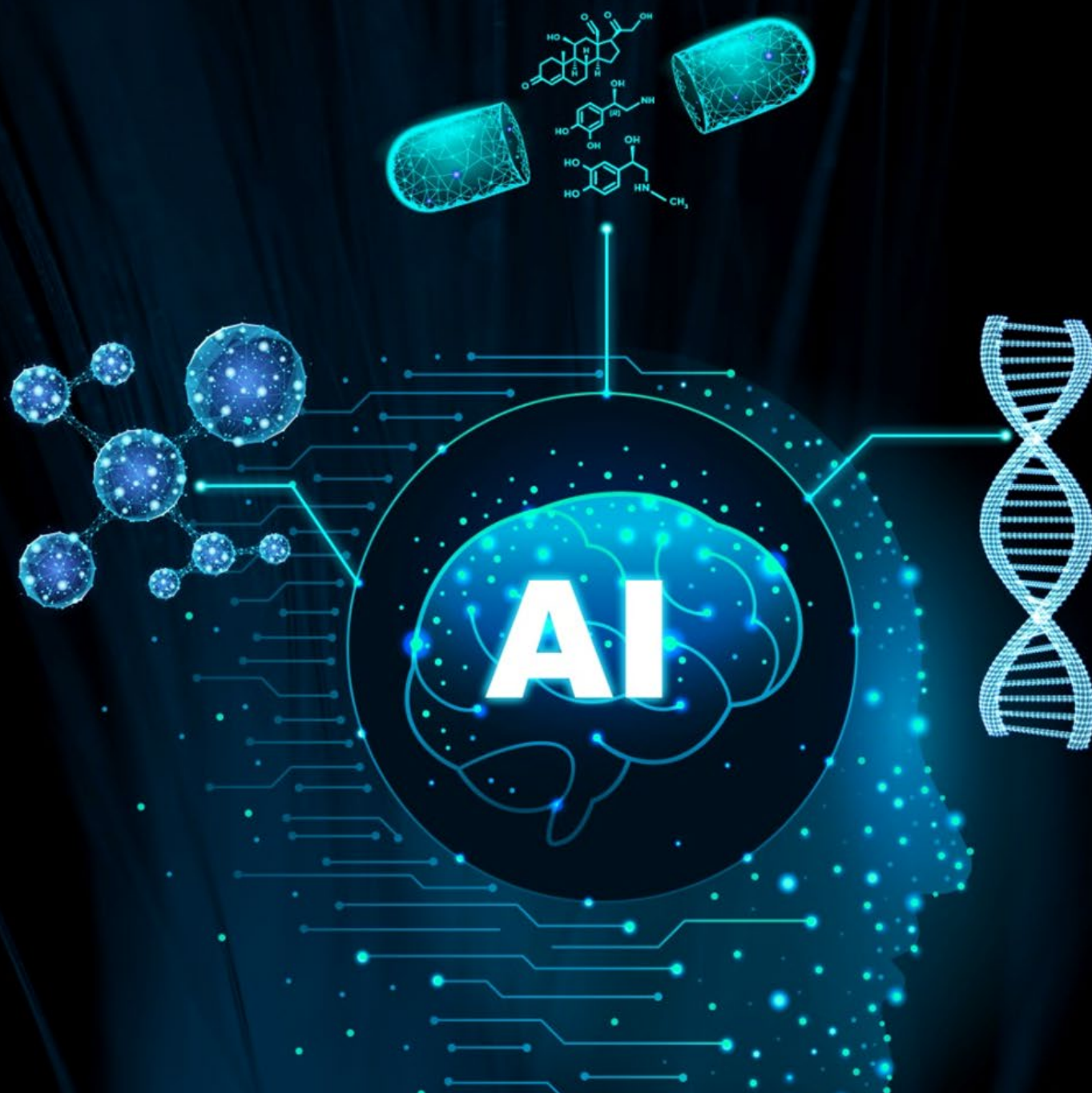


CYBER AIDD

WEEKLY REPORT



CyberAIDD Platform analyzes G-protein-coupled estrogen receptor-mediated 2, 4, 5-trimethylpyridine-3-ols

Derivatives discovery and optimization

Inflammatory bowel disease (IBD) is characterized by an abnormal immune response, including elevated pro-inflammatory cytokines such as tumor necrosis factor- α (TNF- α) and interleukin-6 (IL-6) in the gastrointestinal (GI) tract. In this study, we present the synthesis and evaluation of the anti-inflammatory activity of 2,4,5-trimethylpyridine-3-ol analogues of this class of compounds for TNF- α and IL-6-induced inflammation have a dual inhibitory effect. Based on 3D shape target identification, modeling, and docking, compounds **6-26** were identified as the most effective analogues of G protein-coupled estrogen receptor 1 (GPER). This analogue has shown significant efficacy in improving inflammation and restoring the integrity of the colonic mucosa. This is further validated by the SPR assay results, which show direct binding to GPER, and GPER knockdown is found to eliminate compounds **6-26** inhibition of the effects of TNF- α and IL-6. Notably, compounds **6-26** are non-cytotoxic and are associated with **G1** and **G15** (well-known GPER agonists and antagonists, respectively). Differently, **G1** and **G15** induce necroptosis independent of GPER, respectively. These findings suggest that GPER-selective compounds **6-26** are promising as therapeutic candidates for IBD.

The CyberSAR system played a key role in this study, providing in-depth elucidation of the GPER1 target molecule. The system shows the active molecules associated with the target through the cluster structure view and the original structure view, and presents the potential Hit in the form of a timeline of the R&D stage. In addition, CyberSAR also provides visual analysis of indications and trial design, helping developers quickly obtain target structure information and develop research ideas. Although CyberSAR has not been used in the initial development of molecules, it has shown great potential for application in the elucidation and optimization of drug molecules.

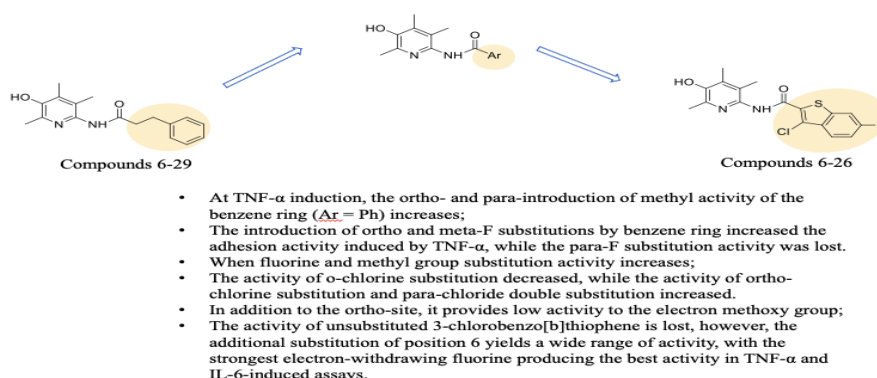


Figure 1 Compound 6-26 discovery and molecular optimization processes



Part II

Inflammatory bowel disease (IBD) is a chronic, recurrent inflammation of the gastrointestinal tract. Based on pathological features, it is broadly divided into two main types: Crohn's disease (CD) and ulcerative colitis (UC). The exact cause of IBD is unknown, and it is thought to be multifactorial. However, deficient immune function of innate and adaptive immunity is a major factor in the pathogenesis of IBD. Although different types of T cells are involved in CD (Th1/Th17-related) and UC (Th2-like), Abnormally high levels of pro-inflammatory cytokines, particularly tumor necrosis factor- α (TNF- α) and interleukins, are key factors in IBD that trigger leukocyte infiltration and subsequent intestinal injury-6 (IL-6) . The intestinal epithelial inflammatory response caused by TNF- α and IL-6 has a common signaling pathway associated with recurrent inflammation and epithelial injury. This pathway is involved in the activation of NF- κ B and STAT3, inducing the expression of various inflammation-related genes, including TNF- α and IL-6. Targeted therapy strategies with anti-TNF- α antibody drugs have been shown to be very effective in the treatment of IBD. These successful developments continue to extend to IL-6 inhibitors, such as anti-IL-6 receptor antibodies (sarilumab). tocilizumab) and anti-IL-6 antibody (stuximab). However, some patients with IBD do not respond to these drugs after an initial or initial response (primary and secondary non-responders). In addition, these expensive antibody therapies can lead to adverse effects, including severe infections, immunosuppression, and lymphoma.

Accumulating evidence suggests that estrogen receptors contribute to the pathogenesis of IBD, similar to their role in other chronic inflammatory diseases such as arthritis, experimental autoimmune encephalomyelitis, systemic lupus erythematosus, and colitis. Epidemiological studies have shown that postmenopausal hormone replacement therapy (HRT) reduces chronic recurrent inflammatory activity in patients with IBD compared with non-HRT users . Estrogen receptor α (ER α) and β (ER β) play an important role in IBD. Hyperexpression of ER β in the IBD colon is reduced, leading to a loss of its anti-inflammatory effects, which is promoted by autophagy and downregulated by P2X7RLead. In addition, the anti-inflammatory effects of estrogen are also linked to estrogen receptor 1 (GPER, also known as GPR30) through G protein, a rapidly regulated membrane-bound receptor Mediating signaling molecules.

The anti-inflammatory effects of GPER have been demonstrated in studies in which GPER knockout in mice resulted in increased plasma inflammatory cytokine levels in mice with chemically induced IBD in GPER. The agonist **G1** improves colitis. GPER has been widely expressed in many cells, including immune cells, brain, heart, kidneys, and intestines. Depending on the cell type, GPER signals through different G proteins, including G α s, G α i, and more G α q/11 and G β γ proteins. In addition to the activation of cAMP and ERK, GPER signaling also interacts with other signaling molecules, such as JAK/STAT3, YAP/TAZ, CREB, Elk1, and NF- κ B. NF- κ B is involved in the gene expression of a variety of pro-inflammatory cytokines, including TNF- α and IL6, which in turn induce phosphorylation through receptor signaling nuclear translocation of STAT3. Studies of NF- κ B and STAT3 knockout or overexpression cells also support TNF- α or IL-6 induction nuclear translocation of NF- κ B and STAT3. NF- κ B and STAT3 are independent of each other. In summary, there is growing evidence that activation of GPER inhibits TNF- α and IL-6 signaling, which is important for refractory IBD. It is an effective treatment strategy for patients.

Previously, using a phenotype-based drug discovery strategy, 6-alkylamide-2,4,5-trimethylpyridine-3-ol was reported in an in vitro IBD model as a result of dual inhibition against TNF- α and IL-6-induced inflammatory activity. Phenylethyl analogue (**6-29**), attached to the benzyl and cyclohexyl side chains of the 6-amide group, exhibits high activity, probably due to the degree of flatness provided by these side chains. In the present study, for better double inhibition, the range of the side chains was expanded to increase their flatness and attach them directly to the amide functional group. In the context of IBD drug discovery, targeting a single molecule may not fully address the multifaceted pathogenesis of the disease. To overcome this problem, the authors established a cell-based screening system. This system mimics colon tissue damage caused by the sustained influx of inflammatory cells, such as monocytes and macrophages, which are predominantly treated by TNF- α or IL-6 (IBD). of pro-inflammatory cytokines) activated. Compounds on cytokine-induced mononuclear U937 macrophages (TPA-treated U937 cells)-epithelial cells (HT-29). The inhibitory activity of adhesion is determined by measuring the fluorescent signal emitted by the attached cells. Then, the GPER was identified as a promising molecular target using CADD, such as alignment, modeling, and docking based on 3D shapes. Direct binding of the compound to GPER was verified by SPR assay and a series of cell function assays.

Research on structure-activity relationship

Compound (**6-01–6-28**) on TPA-treated mononuclear U937 cells (U937 macrophages) and colonic epithelioid HT-29 cells adhesion inhibitory activity is expressed in Table 1 as % inhibition. Adhesion is induced by TNF- α and IL-6. In general, the activity of the adhesion system induced by TNF- α is highly correlated with the activity of the system induced by IL-6.

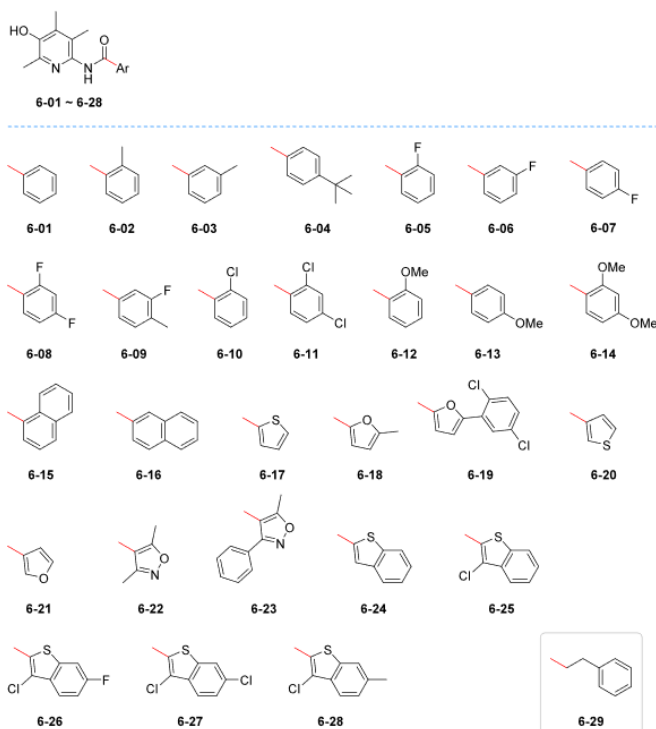


Figure 1. 6-Arylamido-2,4,5-trimethylpyridinol (6-01 to 6-28).

In the assay induced by TNF- α , the benzene ring (Ar = Ph) at **6-01** The ortho and para-introduction of methyl groups increased activity by 2.5-fold and 3.5-fold (**6-02** and **6-03**, respectively).), but not in IL-6-induced systems. The large tert-butyl substituents do not enhance their activity (**6-04**). The introduction of ortho-F and meta-F substituents into the benzene ring makes TNF- α The induced adhesion activity is two- and triple-fold (**6-05** and **6-06**, respectively), while para-F displaces this activity loss. When fluorine and methyl substituents (**6-08** and **6-09**) activity increases. An analogue (**6-05**– **6-09**) with a fluoride substituent shows a TNF- α inducible system and IL-6 There is considerable correlation between the induction systems. In contrast to o-F, o-Cl decreases activity, while ortho- and para-double substitutions increase activity (**6-10** and **6-11**, respectively). Provides low activity to the electromethoxy group unless it is ortho (**6-12** vs **6-13** and **6-14**). In the five- membered aromatic ring, the activity of thiophene-containing analogues is highly dependent on structural chemistry (**6-17** vs. **6-20**), whereas furans are independent of structural chemistry (**6-18** vs. **6-21**) . Isoxazole exhibits very high activity (**6-22**), while the introduction of phenyl substituents decreases activity (**6-23**). Conversely, similar substitutions on the furan ring maintained very high activity (**6-18** vs. **6-19**) . The role of biarylsyl appears to be quite complex (**6-19** and **6-23**), which has led to the exploration of double rings. Naphthalene groups generally exhibit high activity (**6-15** and **6-16**). The activity of unsubstituted 3- chlorobenzo[b]thiophene is negligible (**6-24** and **6-25**). However, the additional substitution of the 6-bit produces a wide range of activity. The strongest electron- withdrawing fluorine yields the best activity in TNF- α and IL-6-induced assays (**6- 26**), reaching 90.3% and 79.2% respectively. IC_{50} values reveal interesting results.

The IC_{50} values for compounds **6-26** were 0.23 μ M (TNF- α inducible assay) and

0.35 μM (IL-6 inducible assay), while the control drug tofacitinib The $_{\text{IC}_{50}}$ values were 0.70 μM and 0.48 μM , respectively. A more significant difference was found when compared to another control drug, mesalazine. In clinical practice, mesalazine is commonly used to treat UC characterized by mild to moderate disease activity. At a dose of 4 g per day, mesalazine exerts a local effect on intestinal epithelial cells, mainly local rather than systemic absorption. Compounds **6-26** produce an $_{\text{IC}_{50}}$ that is almost six orders of magnitude higher than mesalazine. From F>Cl>Me (**6-26**, **6-27**, **6-28**), electron absorption is reduced, Decreased activity. The best analogues (**6-26**) were also compared. With compound **6-29**, **6-alkylamide** analogues, we previously reported as the best pair against TNF- α and IL-6Depressor. In both TNF α and IL-6-induced assays, compounds **6-26** have better inhibitory activity than compounds **6-29**.

Table 1. Inhibitory Activity of Compounds at a 1 μM Concentration against TNF α - and IL-6-Induced Adhesion of Human Monocytic Cells (TPA-Treated U937) to Human Colonic Epithelial Cells (HT-29)

compound	% inhibition at 1 μM concentration	
	TNF α -induced adhesion ^a	IL-6-induced adhesion
6-01	18.5 \pm 8.9	44.1 \pm 9.5 ^b
6-02	47.3 \pm 2.2 ^b	41.5 \pm 6.5 ^b
6-03	63.9 \pm 3.2 ^b	48.9 \pm 10.4 ^b
6-04	22.5 \pm 11.6	29.4 \pm 6.0 ^b
6-05	36.4 \pm 2.7 ^b	66.4 \pm 4.2 ^b
6-06	54.1 \pm 1.4 ^b	44.2 \pm 5.8 ^b
6-07	13.7 \pm 12.8	5.5 \pm 5.4 ^b
6-08	71.4 \pm 4.3 ^b	62.4 \pm 4.3 ^b
6-09	68.2 \pm 14.6 ^b	59.5 \pm 8.3 ^b
6-10	7.9 \pm 2.8 ^b	15.0 \pm 4.8 ^b
6-11	58.6 \pm 4.5 ^b	46.4 \pm 4.9 ^b
6-12	58.0 \pm 3.8 ^b	44.0 \pm 6.9 ^b
6-13	13.9 \pm 6.2	6.5 \pm 6.2 ^b
6-14	30.9 \pm 3.5 ^b	19.1 \pm 6.3
6-15	64.9 \pm 4.1 ^b	56.5 \pm 7.8 ^b
6-16	42.9 \pm 7.4 ^b	33.1 \pm 7.6
6-17	68.4 \pm 2.8 ^b	61.6 \pm 5.8 ^b
6-18	79.9 \pm 1.2 ^b	70.2 \pm 6.4 ^b
6-19	78.2 \pm 3.9 ^b	69.6 \pm 3.7 ^b
6-20	11.5 \pm 3.8 ^b	19.3 \pm 8.0 ^b
6-21	60.3 \pm 0.8 ^b	54.1 \pm 4.5 ^b
6-22	85.0 \pm 8.3 ^b	74.0 \pm 7.0 ^b
6-23	18.8 \pm 7.8 ^b	37.8 \pm 11.2 ^b
6-24	16.5 \pm 4.5	27.0 \pm 7.2 ^b
6-25	13.4 \pm 7.6	11.4 \pm 7.1 ^b
6-26	90.3 \pm 10.1 ^b	79.2 \pm 8.6 ^b
6-27	19.5 \pm 4.1 ^b	9.0 \pm 5.5
6-28	9.1 \pm 5.3	8.7 \pm 7.5
6-29 ⁴³	72.5 \pm 13.2 ^b	69.6 \pm 9.8 ^b
tofacitinib	49.1 \pm 0.1 ^b	58.6 \pm 2.3 ^b
mesalazine	9.9 \pm 14.7 (1 mM)	1.7 \pm 7.8 (1 mM)

^aData are shown as "mean \pm SEM" of at least three independent experiments performed in triplicate. ^b $P < 0.05$ versus vehicle-treated group.

3D).

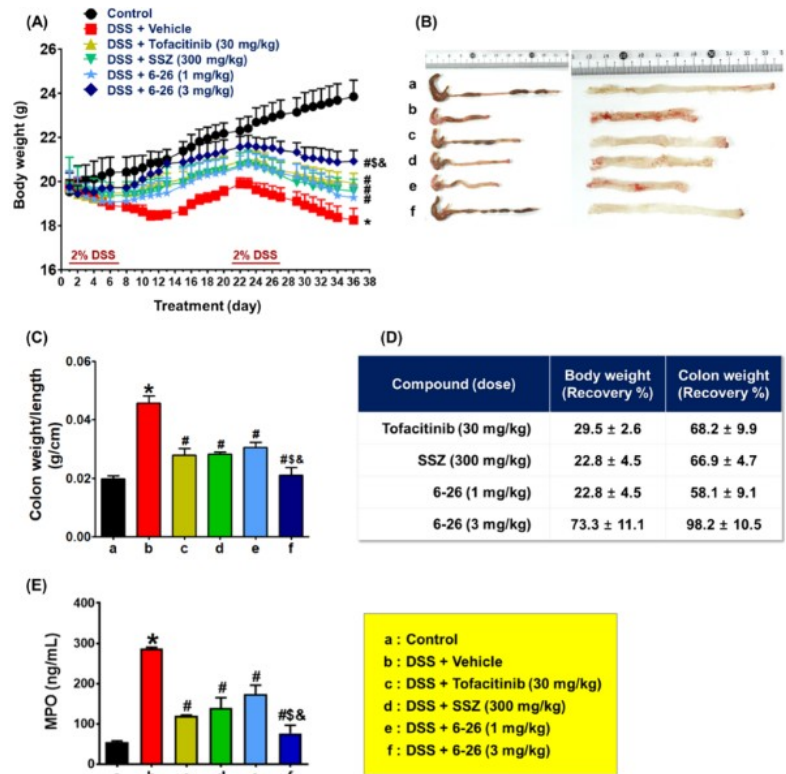


Figure 4. Ameliorating effect of 6-26 on DSS-induced murine chronic colitis ($n = 6$). Chronic type of colitis was induced by two cycles of oral administration of DSS (2 w/v%) dissolved in drinking water for 7 days with an interval of 2 weeks in mice. Drugs, 6-26, sulfasalazine, and tofacitinib, were orally administered daily for 35 days, 6 days per week. (A) Body weight changes. (B) Gross morphology of the colon from cecum to rectum in uncut (left panel) and longitudinal cut section to show mucosa (right panel). (C) Colon weight/length. (D) Recovery rate in body weight and colon weight/length. (E) MPO level in colon tissues was determined by using the MPO assay kit. * $P < 0.05$, compared with the untreated control (Mock) group. # $P < 0.05$, compared with the vehicle-treated DSS colitis group. & $P < 0.05$, compared with the tofacitinib-treated group. & $P < 0.05$, compared with the SSZ-treated group.

In addition, dose-dependent ameliorating activity in a non-chronic and recurrent IBD model of compounds **6-26** was also studied, treated with two cycles of dextran sodium sulfate (DSS) in mice 6 days, followed by 14 days of water. Compound **6-26** orally administered daily for 5 weeks, 6 days a week, significantly blocks DSS induced weight loss (Figure 4A) and colon inflammation, hemorrhagic injury, and length shortening (Figure 4B). Body weight (Figure 4A, D) and colon weight (Figure 4C) for compounds **6-26** D) recovery was dose-dependent and consistent with tofacitinib (30 mg/kg) and SSZ (300 mg/kg). Compounds **6-26** inhibit DSS-induced colonic MPO levels in a dose-dependent manner with a stronger effect than tofacitinib and SSZ (Figure 4E).

Functional healing effect of compounds 6-26 on DSS-induced damage to the colonic mucosa

The dose-dependent mucosal healing effect of compounds **6-26** in the IBD model was further evaluated by assessing changes in intestinal permeability. Intestinal mucosal permeability is a key aspect of intestinal barrier function and is essential for protecting the body from pathogens and toxins and facilitating nutrient absorption. DSS-induced intestinal inflammation disrupts the expression of tight junction-related proteins and impairs the integrity of the epithelial barrier, a hallmark observed in human IBD. This initial disruption can then exacerbate symptoms, including increased permeability, bleeding, and death. In an acute colitis model evaluating the therapeutic effect of compounds **6-26** (Figure 5A), DSS-induced colitis was characterized by erosions, ulcers, crypt loss, and hematoxylin and eosin (H&E). Histopathological examination of the stained tissue is characterized by significant neutrophil infiltration (Figure 5B). However, these pathological changes are severe.

Improvement by compound **6-26** dependence (Fig. 5B, C). Blood samples from the DSS-treated group showed significantly elevated levels of fluorescein isothiocyanate (FITC) dextran (4kDa) administered orally (Figure 5D), while this level is significantly reduced after administration of compounds **6-26** (Figure 5D).

Importantly, the mucosal healing effect of compounds **6-26** exceeded that of the tofacitinib and SSZ treatment groups.

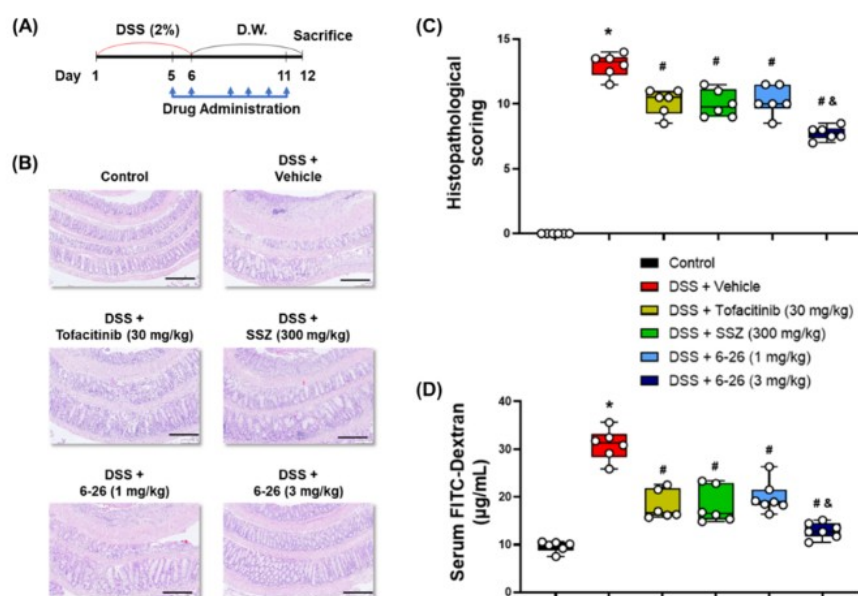


Figure 5. Mucosal healing effect of **6-26** on DSS-induced acute colitis in C57BL/6N/Crl male mice ($n = 6$). (A) Experimental design scheme to confirm the therapeutic effect of compound **6-26** in a DSS-induced acute colitis model. (B) Representative images of histopathological morphology of mouse colon tissues stained with H&E. Scale bar = 200 μ m. (C) Histopathological analysis of H&E-stained mouse colon tissues was assessed based on the predetermined histopathological scoring criteria. $^*P < 0.01$, compared with the untreated control group. $^{\#}P < 0.01$, compared with the vehicle-treated DSS colitis group. $^{\&}P < 0.01$, compared with the SSZ-, tofacitinib-, or **6-26** (1 mg/kg)-treated group. (D) Intestinal permeability was assessed by administering FITC-dextran 4 kDa orally to mice and quantifying the fluorescence intensity in the blood. $^*P < 0.01$, compared with the untreated control group. $^{\&}P < 0.01$, compared with the vehicle-treated DSS colitis group. $^{\#}P < 0.05$, compared with SSZ-, tofacitinib-, or **6-26** (1 mg/kg)-treated group.

In vitro safety assessment

Compounds **6-26** are exposed to five major human hepatic cytochrome P450 (CYP) enzymes at a concentration of 10 μ M, including: CYP1A2, CYP2C19, CYP2D6, CYP2C19, and CYP3A4) were tested. As shown in Table 2, compounds 6-26 appear to be negligible through the potential drug interactions of these major CYP subtypes. In addition, at concentrations of 10 μ M, **6-26** exhibited very weak inhibition of hERG channels (Table 2), Indicates a low risk of cardiotoxicity (e.g., arrhythmias).

Table 2. In Vitro Safety Evaluation of Compound 6-26 at a Concentration of 10 μ M

CYP450 (% control activity)					hERG (% hERG activity)
1A2	2C19	2D6	2C19	3A4	
89.2	99.8	86.0	98.3	89.9	91.7

In vivo acute toxicity studies

To evaluate the safety of compounds **6-26**, **6-26** is administered orally in a single dose of 30 and 300 mg/kg, pairs Acute toxicity studies were performed on ICR mice. After dosing, over the course of 14 days, no weight loss or adverse reactions such as abnormal behavior, food and water intake, and digestive disturbances were observed in the experimental group compared to the control group (vehicle) (Figure 6A).

Subsequently, the mice were euthanized and tissue samples were collected for analysis. Histopathological examination by H&E staining showed no significant tissue damage or inflammatory response in the compound **6-26** groups (Fig. 6B, C) 。 These findings strongly support the sound safety profile of compounds 6-26 and warrant further advancement in drug development efforts.

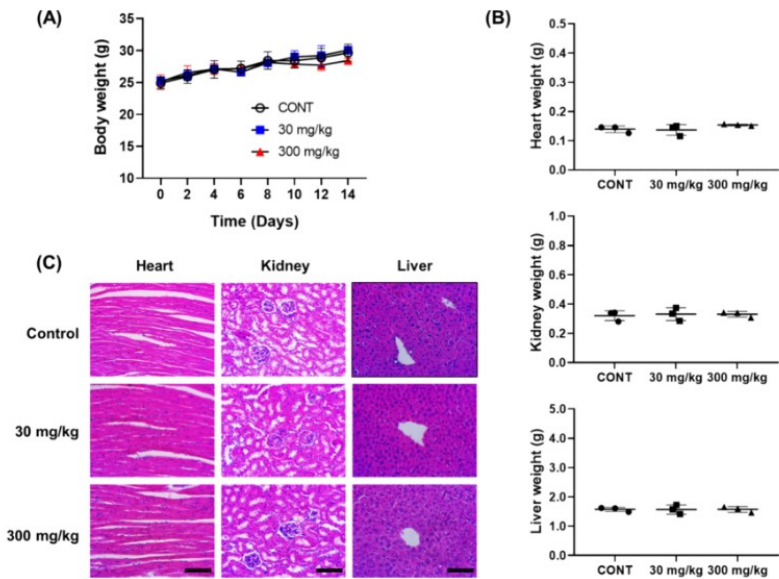


Figure 6. No acute oral toxicity of 6-26 in mice. (A) Mean body weight change. (B) Wet weight of the heart, kidney, and liver. (C) Histology of the heart, kidney, and liver stained with H&E. Scale bar = 100 μ m. All quantitative values were presented as mean \pm SD.

Pharmacokinetic studies

Intravenously (IV, 1 mg/kg) and orally (PO, 1 mg/kg and 5 mg/kg) After dosing, the pharmacokinetic (PK) profile of compounds **6-26** is evaluated in rats. As shown in Table 3, oral administration of **6-26** (5 mg/kg) showed AUC_(0-t) was 1849±714h·ng/mL, MRT_(0-t) is 5.0±0.7h, the half-life is 3.3±0.4h, and the plasma is C_{max} It was 760±684 ng/mL, and the intravenous **6-26** (1 mg/kg) was 1006 ±, respectively 417h·ng/mL, 1.2±0.1h, 2.0±0.6h, and 1880ng/mL. Oral administration of 5 mg/kg showed a bioavailability (F) of 36.7%. AUC showed a significant dose- dependence between oral administration 1 and 5 mg/kg. In summary, it is indicated that **6-26** has good PK characteristics for oral administration.

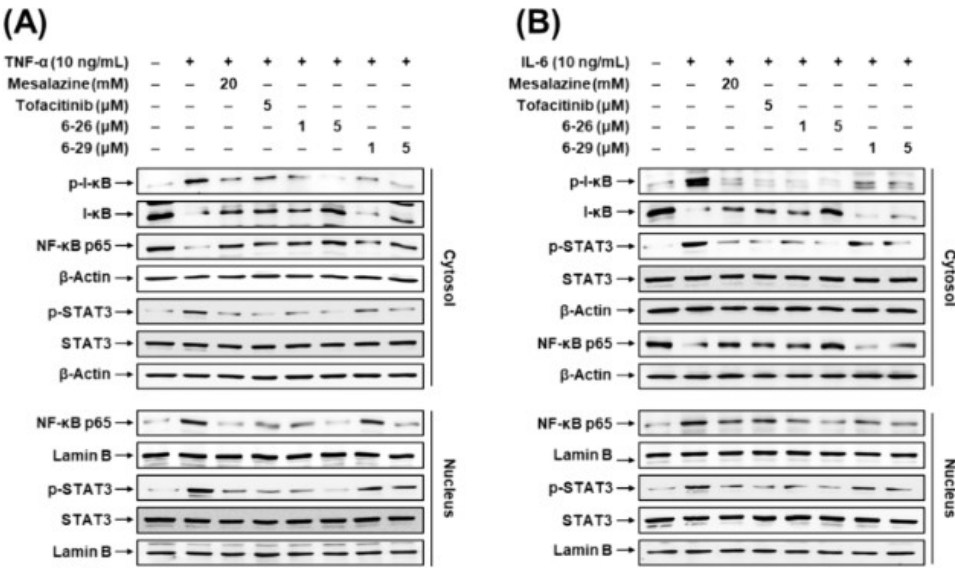
Table 3. Pharmacokinetic Profiles of Compound 6-26 in Rats

parameters / dose	IV at 1 mg/kg	PO at 1 mg/kg	PO at 5 mg/kg
C _{max} (ng/mL)	1880.0	51.9	760.4
AUC _{0-t} (h·ng/mL)	1006.6	246.3	1849.2
V _{ss} (L/kg)	1.3		
T _{1/2} (h)	2.0	3.8	3.3
MRT (h)	1.2	5.7	5.0
CL (mL/min/kg)	17.7		
F (%)		24.5	36.7

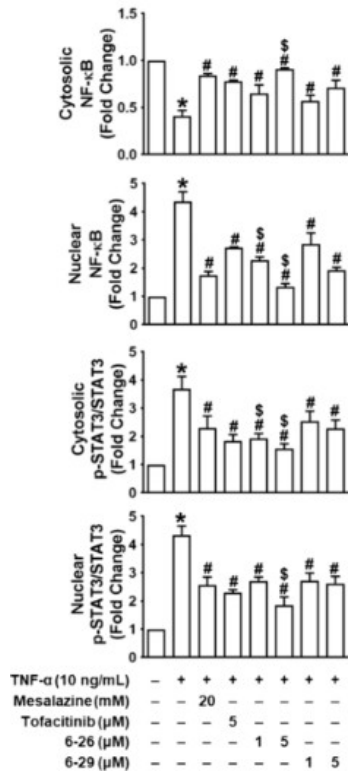
Compounds 6-26 inhibit TNF- α and IL-6 induction NF- κ B and STAT3 nuclear translocation

The cell-level mechanism of action of compounds **6-26** was studied. Since compounds **6-26** inhibit TNF- α and IL-6-induced cellular responses, continue to investigate whether the inhibition of **6-26** correlates with alterations in nuclear NF- κ B and p-STAT3 levels, which are TNFR1Downstream targets of signaling pathways and IL-6 receptors. Although TNF- α and IL-6 are known to increase nuclear NF- κ B and p-STAT3, but the chronological sequence in which each stimulus activates these transcription factors remains unknown. This study first compared TNF- α and IL-6 induction in HT-29 cells Extent of nuclear translocation of NF- κ B and p-STAT3.

After treatment, TNF- α were in 5 min NF- κ Band after 1 h induces p-STAT3 nuclear translocation, while IL-6 is in 5 min to induce p-STAT3 and 30 min to induce NF- κ B nuclear translocation. 1 h after treatment, TNF- α and IL-6 nuclei NF- κ B increased by folds of 7-fold and 4-fold, respectively, while TNF-The fold increase in nuclear p- STAT3 by α and IL-6 is almost similar, both by a factor of 5. These results were further confirmed by immunostaining. Pretreatment of HT-29 cells with **6-26** significantly inhibits TNF- α and IL-6-induced nuclear translocation of NF- κ B and p- STAT3 (Figure 7A). , B) . In TNF- α and IL-6-treated HT-29 cells, **6-26** (1.5 μ M) for NF- κ B and pSTAT3The inhibitory effect of nuclear translocation is greater than that of mesalazine (20 mM) and tofacitinib (5 μ M) (Figure 7C, D) . In addition, this inhibition of compounds **6-26** exceeds that previously reported for compounds **6-29** (Figure 7CD) .



(C)



(D)

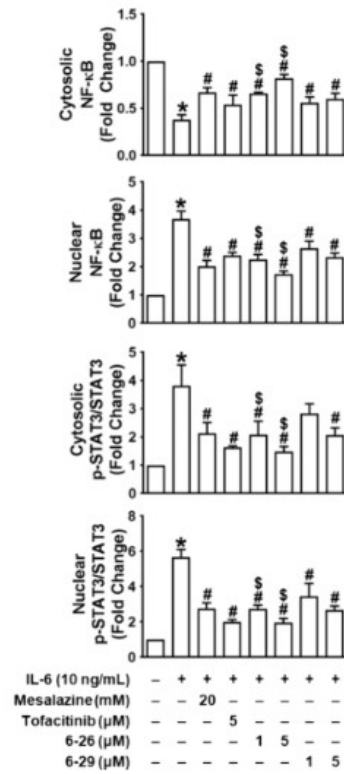


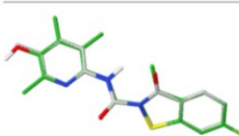
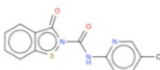
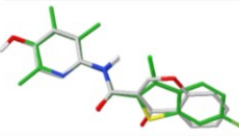
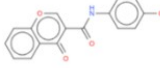
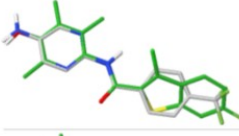
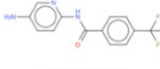
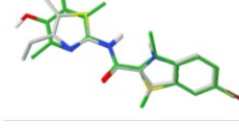

Figure 7. Inhibitory effect of 6-26 on TNF α - and IL-6-induced nuclear translocation of NF- κ B and STAT3. (A, B) HT-29 cells were pretreated with 6-26 and 6-29 for 30 min prior to treatment with TNF α (A) and IL-6 (B) for 1 h. The extracted proteins were analyzed for expressions of pI- κ B/I- κ B, NF- κ B, and p-STAT3/STAT3 in the cytosol and nucleus. The immunoblots are the representative of three independent experiments. (C, D) Quantitation of band intensity in immunoblots. Bar graphs represent the mean \pm SEM. * P < 0.05, compared with untreated cells. # P < 0.05, compared with TNF α - or IL-6-treated group. $^{\$}P$ < 0.05, compared with the 6-29-treated group.

Target identification of compounds 6-26

A variety of methods have been used to predict macromolecular targets for small molecules, such as similarity analysis, machine learning, and docking. These methods are valuable tools for drug discovery, including drug repurposing. Kirchmair's group applied alignment-based methods to identify targets for structurally complex small molecules based on the similarity of 3D molecular shapes to non-complex molecules. They demonstrated that this shape-based approach to target prediction is very robust and successful. Inspired by this work, the authors employed ROCS, a leading shape- based molecular alignment software, to query for matching molecules to bioactive compounds. The IUPHAR/BPS pharmacology guidelines provide an expert-driven knowledge base of drug targets and their ligands, while ChEMBL provides a database of bioactive molecules with drug-like properties. Therefore, the authors searched for a range of drug targets from IUPHAR/BPS and extracted data records of the bioactive molecules for each target from ChEMBL. The threshold pChEMBL value between active and inactive is set to 5.0, corresponding to an IC₅₀ of 10 μ M, EC₅₀ and other relevant measurements. Compounds are normalized by removing salts and charge neutralization, and then molecules with molecular weights less than 250 or greater than 600 are filtered out. If the molecule does not have a well-defined stereochemistry, the stereoisomers are enumerated.

FINALLY, UP TO 50 CONFORMATIONAL ISOMERS WERE GENERATED FOR EACH MOLECULE USING OMEGA.62, FOR A TOTAL OF APPROXIMATELY 26 MILLION CONFORMATIONAL ISOMERS GENERATED FOR THE ACTIVE COMPOUND.

Table 4. Selected Hits from the Shape and Color Alignment of 6-26 to ChEMBL Active Compounds

Alignment	Name	Query	Tanimoto Combo	Shape Tanimoto	Color Tanimoto	Activity
	 CHEMBL3233622	6-26	1.575	0.910	0.665	CASP3 IC ₅₀ = 38.15 nM
	 CHEMBL1814064	6-26	1.510	0.888	0.623	MAOB IC ₅₀ = 64 nM
	 CHEMBL409023	6-26	1.508	0.845	0.663	COX-1 IC ₅₀ = 800 nM
	 CHEMBL4204670	6-26	1.411	0.881	0.531	GPER1 EC ₅₀ = 480 nM

Subsequently, a single 3D conformation of compounds **6-26** was generated using OMEGA. The shape and color properties of compounds **6-26** were then compared to the conformational isomers of the previously generated active compounds. Targets for these hit compounds include caspase-3, NPC1, Sentrin- specific protease, MAOB, and COX-1, carbonic anhydrase, menin, CCR6, PDE7A, HSP90a, S1PR4, GPER1, and S6K-alpha-2. Of these targets, the most relevant phenotypic results observed were caspase-3, MAOB, COX-1, and GPER1 (Table 4). Experiments were then performed to evaluate whether **6-26** inhibited MAOB and COX-1, but they did not exhibit inhibitory effects. The hit compound had the highest ChEMBL3233622 score of 1.575 with caspase-3 inhibitory activity and IC_{50} is 38.15 nM. ChEMBL3233622 belongs to the class of 1,2-benzisothiazol-3-one derivatives, in which the ketone group is one Presence is essential for the binding of caspase-3. **6-26** Lack of ketone groups in the benzothiophene ring; Therefore, caspase-3 activity is not expected to be very strong. Finally, **6-26** also has a high alignment score ChEMBL4204670 with GPER agonists (Tanimoto Combined Score = 1.411), which has an EC_{50} value of 480 nM. The 3D alignment of **6-26** and ChEMBL4204670 calculated using ROCS is shown in the figure 8A shows a rough correspondence between the benzothiophene ring of **6-26** and the indole ring of ChEMBL4204670. The overlap between these compounds can be further distinguished into shape and color components (Figure 8B), indicating that the contribution of shape components is greater than that of color.

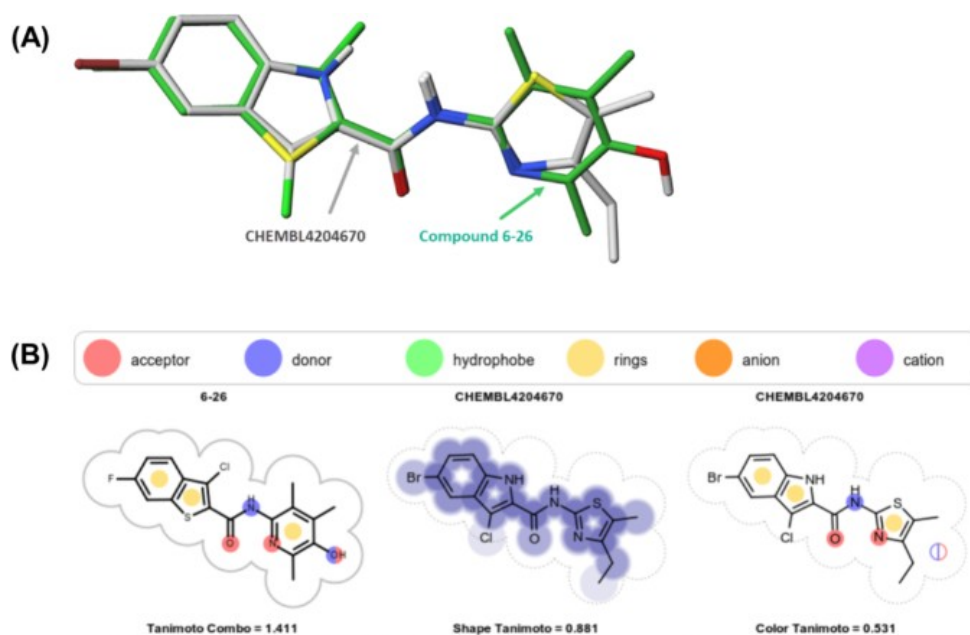


Figure 8. (A) 3D alignment of **6-26** and ChEMBL4204670. (B) 2D schematic representation of the shape and color alignment of **6-26** to ChEMBL4204670.

Compounds 6-26 docking experiments with GPER

6-26 was investigated to see if it could bind to GPER via protein-ligand docking. A 3D model of human GPER generated by AlphaFold (AF-Q99527-F1-model_v4) was obtained from the AlphaFold protein structure database. The CAVIAR is used to identify the binding site and a binding cassette is set up to enclose the cavity. Use Flare 6.0 to dock **6-26** into this binding cavity. The ΔG of the optimal binding posture was -9.9 kcal/mol, indicating that **6-26** had a strong binding interaction with GPER. In the binding posture shown in Figure 9, the main interaction appears to be the π - π interaction between Phe208 and benzothiophene. This bonding posture is consistent with the bonding posture proposed by the Arnatt group.

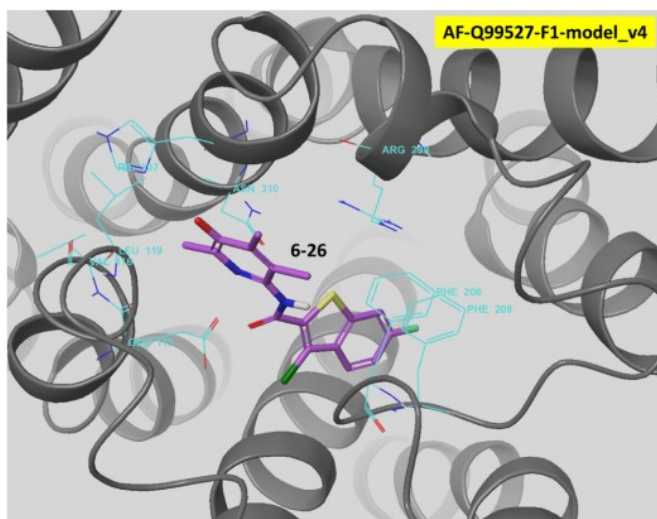


Figure 9. Binding pose of the complex formed between GPER and **6-26**. AlphaFold-generated 3D structure of GPER was used for docking. The π - π interaction between the phenyl ring of Phe208 and the benzothiophene ring of **6-26** is predicted to be the primary binding interaction.

Compounds **6-26** bind directly to the GPER

For the molecular target of **6-26**, the direct binding of **6-26** to human GPER protein was studied by SPR. A sensing plot describing the binding dynamics is shown in Figure 10. The data analysis showed that **6-26** had binding affinity for GPER, and the K_D value was $2.37 \times 10^{-8} \text{M}$. The reliability of the SPR data is measured by χ^2 and U values. In the experiment, a satisfactory $\chi^2(< \text{rmax})$ was obtained (5%) and U values, which demonstrate the validity of the fitting curve and the uniqueness constant of the calculation rate. In summary, the SPR data strongly supports the idea that **6-26** is directly combined with GPER.

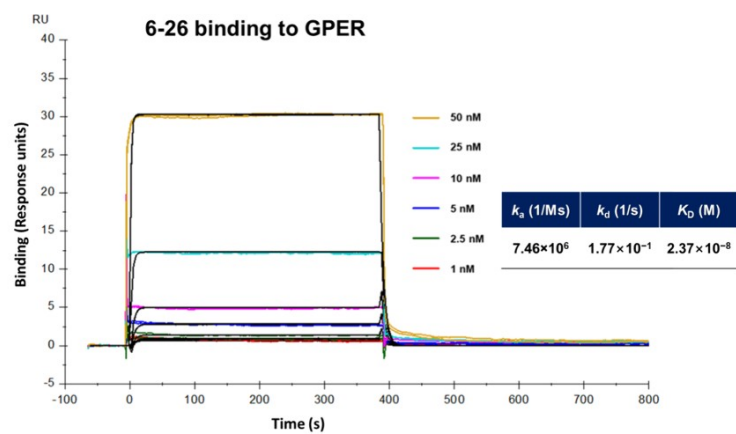


Figure 10. Binding analysis by SPR sensorgram of 6-26. A series of concentrations are shown in different colors. Black lines are fitted curves from kinetic fitting using a 1:1 binding model. The Biacore T200 Evaluation Software was used to determine both k_d (dissociation constant) and k_a (association constant) values. The K_D (equilibrium constant) values were subsequently calculated from the obtained k_d and k_a values.

Compounds 2-26 act on the GPER to perform functions

To further validate GPER as a molecular target for compounds **6-26**, initiate the study by comparing GPER expression levels in model cells of our screening system. Notably, U937 cells exhibit higher levels of GPER mRNA expression than HT-29 cells, and this expression is not affected by TNF- α or the impact of TPA treatment. Compounds **6-26** against TNF- α -induced NF- κ B and p-STAT3. The inhibition of nuclear translocation was similar to that observed with **G1** (GPER agonist) and was reversed by **G15** (GPER antagonists) (Figure 11A). Similarly, in U937 macrophages, **6-26** respond to TNF- α -induced inflammatory genes (e.g., TNF- α , IL-6, IL-1 β , and COX-2) expression was enhanced by **G1** but by **G15** blocks (Figure 11B,C) and HT-29 cells (Figure 11B) in a concentration-dependent manner, **D**). In addition to its anti-inflammatory activity, **6-26** exhibits mucosal healing effects through E-cadherin repair, and this effect is also enhanced by **G1** in a concentration-dependent manner and by **G15** Offset (Figure 11B, D). In addition, FITC-dextran leakage through the HT-29 monolayer showed increased epithelial permeability induced by TNF α , **G1** and **6-26** were mitigated, but **G15** was not mitigated (figure 11E). When treated in combination with **G1** or **G15**, **G1** enhances the protective effect of **6-26**, but: **G15** weakened. In addition, TNF- α was detected by flow cytometry analysis of apoptosis and necrosis, and in HT-29 and U937 macrophages, compounds **6-26** were detected Inhibited -induced cell damage.

However, **G1** did not attenuate TNF- α -induced cell death; On the contrary, it exacerbates the situation. Interestingly, similar to **G1**, **G15** also exacerbates the cytotoxic effects of TNF- α (Figure 11F). Since the results show that **G1** and **G15** themselves have cytotoxic activity, each compound continues to be evaluated at 1 to 10 μ M Cytotoxic effects in the concentration range. These concentrations are known to exhibit potent anti-inflammatory activity in the absence of TNF- α , as previously

reported. Treat HT-29 (Figure 11G) and U937 with **G1** or **G15** alone Macrophages (Figure 11H) induce a concentration-dependent decrease in the number of viable cells and an increase in the dead cell population, where **G1** is more than **G15** with a greater effect (Table 5). In contrast, treatment with compounds **6-26** alone does not induce cell death. **G1** and **G15**-induced cell death was found to be necroptotic via receptor interaction serine/threonine protein kinase 1 (RIP1), RIP3, and mixed-lineage kinase domain-like proteins (MLKLs) to demonstrate that they are hallmarks of necroptosis (Figure 11I). The results showed that the inducible activity of necroptotic **G1** and **G15** was not related to GPER. Combined with the results of previous studies, attributing the cytotoxic effects of **G1** to cytoskeletal disruption, independent of its interaction with GPER, the current findings suggest that **6-26** is the ratio **G1** or **G15** are safer and more selective GPER compounds.

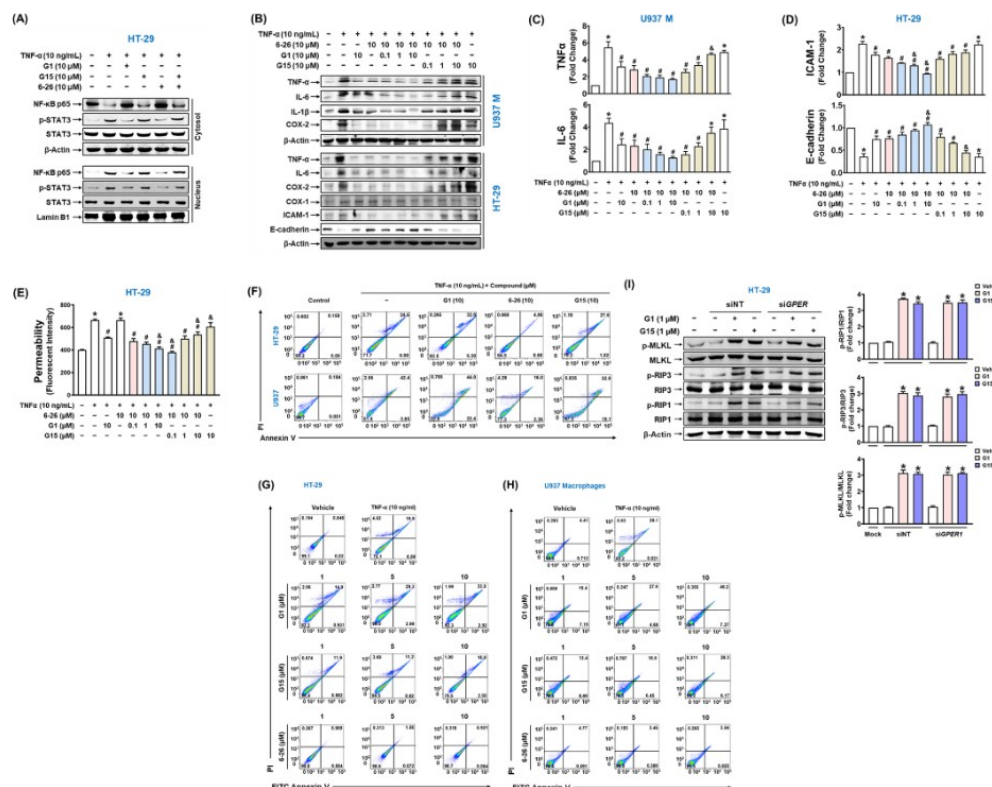


Figure 11. Inhibitory effect of 6-26 on TNF α -induced inflammatory gene expression and cell death was mediated through GPER. (A–D) Cells were cotreated with 6-26 and G1 or G15 prior to TNF α treatment for 3 h. The immunoblots showing nuclear transcription factors (A) and gene expressions (B) are representative of three independent experiments. Quantification of the band intensity from the immunoblots of inflammatory cytokines in U937 macrophages (C) and cell adhesion-related molecules in HT-29 cells (D) was performed. Bar graphs represent mean \pm SEM. * P < 0.05, compared with untreated control cells. # P < 0.05, compared with the TNF α alone-treated group. & P < 0.05, compared with the combination (TNF α plus 6-26)-treated group. (E) Paracellular permeability was measured in 7-day cultured HT-29 cells. After the monolayer of HT-29 cells was cotreated with 6-26 and G1 or G15 prior to TNF α treatment for 3 h, FITC-dextran (4 kDa) was loaded in the upper chamber. After 2 h, fluorescence intensity in the lower chamber was determined. * P < 0.05, compared with untreated control cells. # P < 0.05, compared with the TNF α alone-treated group. & P < 0.05, compared with combination (TNF α plus 6-26)-treated group. (F–H) Flowcytometric measurement of apoptotic and necrotic cell death after the drug treatment for 24 h in the presence (F) or absence (G, H) of TNF α . * P < 0.05, compared with control cells. # P < 0.05, compared with the TNF α alone-treated group. & P < 0.05, compared with the combination (TNF α plus 6-26)-treated group. (I) Immunoblots showing activation of RIP1, RIP3, and MLKL, the necroptosis markers, in HT-29 cells transfected with GPER siRNA or treated with chemicals (G1 or G15). GPER knockdown did not induce activation of RIP1, RIP3, and MLKL, nor did it affect G1- or G15-induced necroptotic cell death. * P < 0.05, compared with the vehicle-treated control group. # P < 0.05, compared with siNT-treated group.

Adhesion assays are performed on GPER-silenced cells, further confirming that GPER is a target for 6-26. 6-26 pairs of TNF- α -induced (Figure 12A) and IL-6- induced (Figure 12A). 12B) adhesion effect is comparable to that of G1. When 6-26 is combined with G1, the inhibition effect of 6-26 is slightly better than that of G1 alone, while G15 significantly blocks the inhibition effect of 6-26 (Fig. 12A, B). 6-26 cytokine-induced inhibition in HT-29 cells by GPER with siRNA knockdown to eliminate adhesion, TNF- α treatment compared to non-target siRNA transfection (Figure 12C) The inhibition effect of 6-26 was reduced by 73%, and the case of IL-6 treatment (Fig12D) reduced by 78%. In addition, GPER knockdown in HT-29 and U937 macrophages (Figure 12E) eliminated compounds 6-26 inhibits 88% of TNF- α - induced adhesion (Figure 12F). These results strongly support the conclusion that GPER is indeed the target of 6-26.

Conclusion

This study highlights the potential therapeutic importance of compounds **6-26**, a novel GPER-targeted compound that works by inhibiting key signaling pathways and pro-inflammatory Expression of molecules, specifically TNF- α and IL-6, to disrupt the vicious cycle of inflammation for the treatment of IBD. At the cellular level, compounds **6-26** exhibit dual modes of action, including anti-inflammatory properties and tissue repair capabilities. This dual effect has been observed in both macrophages and colonic epithelial cells. In animal models representing acute and chronic IBD, compounds **6-26** have shown significant efficacy in relieving colitis and promoting mucosal healing. Molecular modeling and target prediction showed that GPER was a specific molecular target for compounds **6-26**. This hypothesis was validated by SPR direct binding experiments and by GPER agonists (**G1**) and antagonists (**G15**).) and molecular gene silencing experiments further confirmed. All of these experiments confirmed that the effects of compounds **6-26** in inhibiting inflammation and restoring the intestinal epithelial barrier were mediated by GPER. Compounds **6-26** activate GPER, which is a major regulator of inflammation reduction and epithelial recovery. In addition, this study showed that **G1** and **G15** induce necrotizing cell death independently of GPER, while 6-26 do not exhibit cytotoxicity, rather, it exerts a protective effect on TNF- α -induced necroptosis. The 100-fold safety assessment of compound **6-26** was strongly supported by the fact that the dose above the effective dose did not show significant tissue damage or inflammatory response. In conclusion, compounds **6-26** play a key regulatory role in inflammation and epithelial repair through GPER activation. This GPER-targeted compound **6-26** has the potential to be used as a first-line treatment for patients with IBD, as well as a new, safer treatment option for patients who do not respond well to current treatments or experience side effects. Further clinical studies are needed to explore the translational potential of **6-26** pairs in patients with IBD.

Article source: <https://doi.org/10.1021/acs.jmedchem.3c02458>

Part III

1. Combined with drug design ideas, the structure of the activity reported in the literature and patents was excavated CyberSAR facilitates the rapid acquisition of target structures of interest to developers for the development of ideas on **G-protein coupled estrogen receptor 1 (Homo SAPIENS)** are examples below:

GP1 : G-protein coupled estrogen receptor 1 (Homo sapiens)

- Structure Info
- Indication
- ChemSpace
- Assay Data
- Bioassay
- SAR Doc

Target Landscape

Name	G-protein coupled estrogen receptor 1
Synonyms	<div>G蛋白偶联雌激素受体1</div> <div>FEG-1</div> <div>mER</div> <div>Flow-induced endothelial G-protein coupled receptor 1</div> <div>Membrane estrogen receptor</div> <div>GPCR-Br</div> <div>Lymphocyte-derived G-protein coupled receptor</div> <div>Chemoattractant receptor-like 2</div> <div>IL8-related receptor DRY12</div> <div>G-protein coupled receptor 30</div> <div>G protein-coupled estrogen receptor 1</div> <div>LYGPR</div>
Organism	Homo sapiens
Class	<div>-</div> <div>Membrane receptor</div> <div>Family A G protein-coupled receptor</div> <div>Small molecule receptor (family A GPCR)</div> <div>Lipid-like ligand receptor (family A GPCR)</div> <div>Steroid-like ligand receptor</div>
Type	SINGLE PROTEIN
Ext. Links	<div>GenCards</div> <div>OpenTarget</div> <div>UniProt</div> <div>PDB</div> <div>AlphaFold</div>
Physiological Function	G-protein coupled estrogen receptor that binds to 17-beta-estradiol (E2) with high affinity, leading to rapid and transient activation of numerous intracellular signaling... <div>More</div>

3D Structure

With Ligands

Others

8XQJ (PDB)

8XOI (PDB)

8XOH (PDB)

8XOG (PDB)

8XOF (PDB)

Sequence

Q99527 (Uniprot)

Uniprot ID	Q99527	MD5	1af95f3749986237561fb006bbc74da2
Length	375		Download Fasta File
<div><div>102030405060708090100110120130</div><div>MDVTSQARGV GLEMYPGTAQ PAAPNTTSPE LNLSHPLLGT ALANGTGELS EHQQYVIGLF LSCLYTIFLF PIGFVGNILI LNVNIFREK MTIPOLYPIN LAVADLILVA DSLIEVFNH ERYDIAVLC</div><div>140150160170180190200210220230240250260</div><div>TFMSLFLOVN MYSSVFLLTW MSFDRIYALA RAMRCSLFRT KKHARLSCGL INMASVSATL VPFTAVHLQH TDEACFCFAD VREVQWLEVT LGFIVFFAII GLCYSLIVRV LVRARRHRL RPRRQKALRM</div><div>270280290300310320330340350360370</div><div>ILAVVLVFFV CWLPENVFIS VHLLQRTQPG AAPCKQSFRI AHPLTGHIVN LAAFSNSCLN PLIYSFLGET FRDKLRLYIE QKTNLPALNR FCHAALKAVI PDSTEQSDVR FSSAV</div></div>			

2. At the target interface, select the "Chemical Space" option under the "Clustering Structure View" tab, and you can display the molecules related to GPER in the literature and patents collected by the CyberSAR platform in the form of "core structure clustering". The green font highlights the "EC50 < 1000 nM or IC50 < 1000 M" of the active molecule structure, specific experiments, experimental results, and experimental sources reported in vitro enzyme, cell activity test experiments.

GPER1 : G-protein coupled estrogen receptor 1 (Homo sapiens)

Structure Info
Indication
ChemSpace
Assay Data
Bioassay
SAR Doc

Target Landscape

Real Structure Cluster Structure (12) Clustering Threshold Loose Strict

Tips: 1- The chemical space includes molecules labeled manually and those identified through experimental data mining; 2- Manual labels are sourced from the Pharmacodia global drug database and other manually confirmed sources; Active molecules are those with activity indicators ≤1000nM; 3- The R&D status reflects the highest development status of the molecules contained in the cluster.

CC331445	CC642971	CC643428	CC644755
Clustered Mol: 887 Active Mol: 1 Clinical Mol: 30 (Approved)	Clustered Mol: 460 Active Mol: 0 Clinical Mol: 2 (Approved)	Clustered Mol: 45 Active Mol: 3 Clinical Mol: 1 (Phase 3 Clinical)	Clustered Mol: 107 Active Mol: 1 Clinical Mol: 0

Pharmacodia Global

Assay Data | CC331445 13 Results

Filter Sort Default DES Page Size 10

Home > Target Overview > Target

GPER1 : G-protein coupled estrogen receptor 1 (Homo sapiens)

Structure Info
Indication
ChemSpace
Assay Data
Bioassay
SAR Doc

Target Landscape

Estradiol transdermal Approved	Estradiol transdermal Approved	Estradiol transdermal Approved	Estradiol transdermal Approved
Activity = 3 % Displacement of 1-[2-[4-(6-bromobenzo[1,3]dioxol-5-yl)-3a,4,5,9b-tetrahydro-3H-cyclopenta[c]quinolin-8-yl]ethyl]-3-(3-iodo[125]-phenyl)urea from 10.1021/jm9011802	Activity < 10 % Antagonist activity at GPR30 in human SKBR3 cells assessed as inhibition of estradiol-induced calcium mobilization at 10 uM 10.1021/jm9011802	Activity < 10 % Antagonist activity at GFP-tagged GPR30 expressed in COS7 cells assessed as inhibition of estradiol-induced PI3K activation at 10 uM by 10.1021/jm9011802	Activity = 80 % Agonist activity at GFP-tagged GPR30 expressed in COS7 cells assessed as PI3K activation at 10 uM by PIP3 localization based PH-RFP reporter gene 10.1021/jm9011802
Activity = 100 % Agonist activity at GPR30 in human SKBR3 cells assessed as stimulation of 10.1021/jm9011802	EC50 = 0.3 nM Agonist activity at GFP-tagged GPR30 expressed in COS7 cells assessed as half life for increase in intracellular 10.1021/jm9011802	EC50 = 0.3 nM Agonist activity at GPR30 (unknown origin) by calcium mobilization assay 10.1021/jm9011802	Efficacy = 75 % Agonist activity at G-protein coupled estrogen receptor (unknown origin) expressed in CHO cells at 10 uM after 90 10.1021/jm9011802

https://www.google.com/search?scas_esv=7834d5f5cc440713&q=cascade+syn...

3. Selecting the "Chemical Space" tab subsequently linked to the "Original Structure View" tab in the target interface allows the Display of molecules in the CyberSAR platform with GPER-related experimental test activity based on "development status." The word "data mining" highlighted in green is potential hit.

Home > Target Overview > Target Detail

GP1R1 : G-protein coupled estrogen receptor 1 (Homo sapiens)

Structure Info

Indication

ChemSpace

Assay Data

Bioassay

SAR Doc

Target Landscape

Real Structure (35) | Cluster Structure (12)

Data Range | Manual Label | Data Mining

Download

Tips: 1- The chemical space includes molecules labeled manually and those identified through experimental data mining; 2- The R&D status reflects the highest development status of the molecules.

Approved (1)
Manual Label 0
Data Mining 1

Phase 3 Clinical (1)
Manual Label 1
Data Mining 0

Preclinical (33)
Manual Label 29
Data Mining 4

Estradiol transdermal
Assay Data

LNS-8801
Assay Data

C845656
Assay Data

C845586
Assay Data

C982465
Assay Data

C252763
Assay Data

To Explore Cyber-AIDD further Login on your computer using the below Link

<https://cyber.pharmacodia.com/#/homePage>

If you need further assistance contact us,

For a free trial, Contact Us on

Anil Ranadev
+91 9742627845
anil_ranadev@saspinjara.com

Aravind
+91 9619076286
aravind.p@saspinjara.com

Sachin Marihal
+91 9538033363
sacin.marihal@saspinjara.com

Chetan S
+91 7022031061
chetans@saspinjara.com